



# Effect of friction on corrosion behaviors of AISI 304 and Cr26Mo1 stainless steels in different solutions

Z.X. Dai<sup>1,2,3</sup> · S.L. Jiang<sup>1,2,3</sup> · L.K. Ning<sup>1,2</sup> · X.D. Xu<sup>4</sup> · S. Li<sup>1,2,3</sup> · D.L. Duan<sup>1,2,3</sup>

Received: 25 August 2022 / Revised: 13 October 2022 / Accepted: 14 November 2022  
© China Iron and Steel Research Institute Group Co., Ltd. 2023

## Abstract

The corrosion and tribocorrosion behaviors of AISI 304 austenitic stainless steel and Cr26Mo1 ultrapure high chromium ferrite stainless steel in 3.5 wt.% NaCl and 0.5 mol/L H<sub>2</sub>SO<sub>4</sub> solutions were investigated. Microelectrode electrochemical measurement technology was applied to identify electrochemistry behaviors during tribocorrosion tests in situ. The surface morphologies and compositions of the wear tracks were analyzed by scanning electron microscopy and Raman spectrum. The results showed that compositions of stainless steels, corrosive mediums and applied loads have great influence on tribocorrosion behaviors of stainless steels. Firstly, the corrosion resistance in static state of stainless steels primarily dominates its tribocorrosion behavior; meanwhile, better mechanical properties are in favor of tribocorrosion resistance. Secondly, the corrosion rate is promoted significantly in 3.5% NaCl solution by friction, while the tendency is inconspicuous in 0.5 mol/L H<sub>2</sub>SO<sub>4</sub> solution. Last but not least, passive films on stainless steels can be wiped off by small friction force. With the increase in applied load, the effect of friction converts to forming friction oxide film from removing passivation film, so that a critical load exists below which the friction force can promote the corrosion process extremely.

**Keywords** Tribocorrosion · Stainless steel/PEEK friction pair · Corrosive medium · Applied load · Microelectrode probe

## 1 Introduction

As the most frequently moving parts in the process industry, control valves are widely used in many fields, e.g., petroleum, chemical, coal, energy, etc. When the working medium is corrosive gas or liquid with high

temperature and high pressure, the control valve is prone to leakage, which not only causes a waste of raw materials, but also causes serious pollution to the environment, and even causes fire, explosion, poisoning and other life-threatening safety accident. Therefore, researchers paid more attention to the sealing problem of valves recently. The sealing of the control valve relies on the close contact state between the valve stem and the packing. However, due to the cyclic opening and closing of the valve, the friction between the valve stem and the packing causes wear problems, which is an important reason for the leakage of the control valves [1, 2].

Control valves often serve in corrosive mediums, which means its failure is different from pure wear. Material failure caused by corrosion and wear is called corrosive wear [3, 4]. Pitting, peeling, cracks and scratches can be formed on the surface of the valve stem due to the interaction between the valve stem and packing under corrosive wear condition [5–8]. The damage of the valve stem will further increase the wear of the packing, leading to early leakage.

✉ S.L. Jiang  
sljiang@imr.ac.cn

✉ D.L. Duan  
duandl@imr.ac.cn

<sup>1</sup> Shi-Changxu Innovation Center for Advanced Materials, Institute of Metal Research, Chinese Academy of Sciences, Shenyang 110016, Liaoning, China  
<sup>2</sup> School of Materials Science and Engineering, University of Science and Technology of China, Hefei 230026, Anhui, China  
<sup>3</sup> Liaoning Key Laboratory of Aero-engine Materials Tribology, Institute of Metal Research, Chinese Academy of Sciences, Shenyang 110016, Liaoning, China  
<sup>4</sup> AnSteel LISCO Stainless Steel Co., Ltd., Guangzhou 510760, Guangdong, China

**Table 1** Chemical composition of AISI 304 and Cr26Mo1 stainless steels (wt.%)

Stainless steel	C	Cr	Ni	N	Mo	Nb	Fe
AISI 304	0.035	18.04	8.05	0.054	–	–	Balance
Cr26Mo1	0.0038	25.78	–	0.003	1.00	0.15	Balance

**Table 2** Mechanical properties of AISI 304 and Cr26Mo1 stainless steels

Steel	Hardness/ HRB	Elastic modulus/ GPa	Shear modulus/ GPa
AISI 304	81.8	198.8	76.1
Cr26Mo1	89.0	213.3	86.8

Usually for control valves polymer materials, polymer composites, graphite, etc., are used as seal packings, while stainless steels are used as valve stems. For the tribocorrosion behavior of stainless steels, scholars were concentrated on the damage of stainless steels rubbing with ceramic friction pairs in different corrosive media and proposed some optimization methods in the past [7, 9–12]. In recent years, scholars paid more attention to the tribocorrosion behavior of stainless steels coupled with polymer materials in seawater, focusing on the damage mechanism of polymers in the tribocorrosion condition [13–16]. However, the research on the damage mechanism of stainless steel coupled with polymers under the tribocorrosion condition is insufficient.

The tribocorrosion behavior of the friction pair in control valve must be closely related to the surface state of the stainless steel. Therefore, studying the response of the surface state of stainless steel under different tribocorrosion conditions is significant for understanding the damage mechanism of stainless steel/polymer friction pairs. The tribocorrosion process is accompanied by the removal and regeneration of the passive film on stainless steel at the friction interface [17]. With the combination of electrochemical measurement technology and wear test, the state of the passive film on friction interface could be understood easily [18, 19]. Some models have been proposed to measure or calculate the tribocorrosion rate of passive metals under corrosive wear conditions [17, 20, 21]. However, due to the large difference in the repair speed of the passive film under different conditions and a greater impact of applied potential on the surface state, it is difficult to obtain an accurate tribocorrosion rate from these models. At the same time, the electrochemical signal obtained based on the mixture of the internal and external wear scar, which makes it difficult to recognize the electrochemical behavior inside the wear scar separately.

The microelectrode electrochemical measurement technology is a new type of method with the dimension between the macroscopic classic electrochemical technology and the micro-area scanning probe technology [22]. The microelectrode is used as an independent probe to measure the electrochemical signal at a certain point in the wear scar and accurately obtain the corrosion component. At the same time, the interaction mechanism between tribocorrosion is explored in combination with microscopic morphology.

Austenitic stainless steel has good corrosion resistance and is usually selected as the valve stem material. High-purity ferritic stainless steel is a novel development direction of stainless steel. In this area, ultrapure high chromium ferrite stainless steels developed by Institute of Metal Research, Chinese Academy of Sciences, in recent years have good corrosion resistance together with high strength, which have great application potential [23–25].

In this study, AISI 304 stainless steel and Cr26Mo1 ultrapure high chromium ferrite stainless steel with polyether-ether-ketone (PEEK) friction pair were investigated as the research object. Microelectrode electrochemical measurement technology is used to study their tribocorrosion behavior under different conditions, which is beneficial to discovering the damage mechanism of stainless steels and thus guides the selection of stainless steel/polymer sealing materials in the industry.

## 2 Experimental materials and method

### 2.1 Materials

AISI 304 stainless steel used in this study was supplied by AnSteel LISCO Stainless Steel Co., Ltd., while Cr26Mo1 ultrapure high chromium ferrite stainless steel was developed by Institute of Metal Research, Chinese Academy of Sciences, China. Both of them were in annealing state. Their chemical compositions and mechanical properties are listed in Tables 1 and 2, respectively.

Their metallographic structures are illustrated in Fig. 1. The microstructure of AISI 304 steel is equiaxed austenite grains with twins and inclusions enriched at the grain boundaries. For Cr26Mo1 stainless steel, it shows equiaxed ferrite grains. Due to its ultralow carbon content and

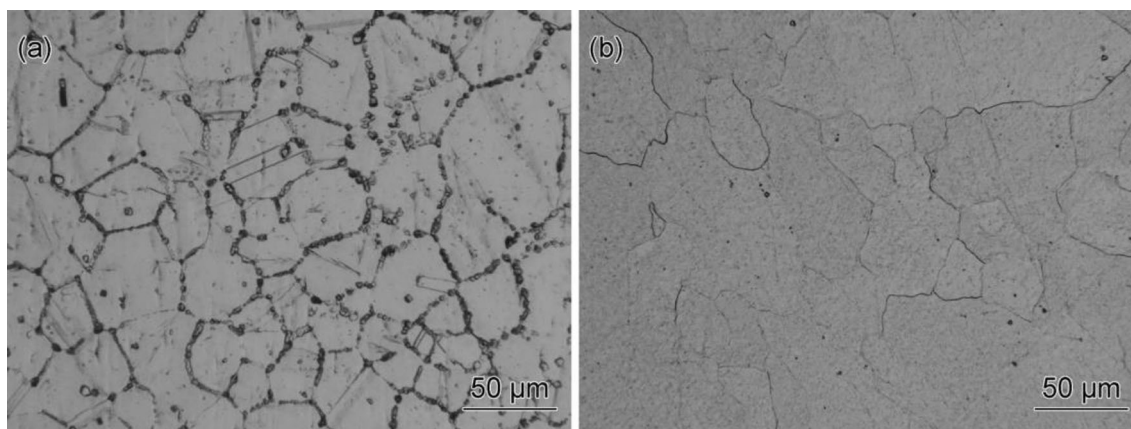


**Fig. 1** Metallographic structure of AISI 304 (a) and Cr26Mo1 (b) stainless steels

nitrogen content, there are few inclusions at the grain boundaries.

## 2.2 Static electrochemical measurements

The samples with the size of 10 mm × 10 mm × 5 mm for electrochemical measurements were polished by 1200-grit silicon carbide paper. The exposed working area was 1 cm<sup>2</sup>. All electrochemical measurements were performed with a standard three-electrode system. The counter electrode was a Pt plate, and a saturated calomel electrode (SCE) with a Luggin capillary was used as the reference electrode. The measurements were performed by using Gamry Reference 600 + electrochemical workstation at room temperature in 3.5 wt.% NaCl and 0.5 mol/L H<sub>2</sub>SO<sub>4</sub> solutions. Electrochemical impedance spectroscopy (EIS) measurement was performed at the open circuit potential (OCP) with an AC signal of amplitude 10 mV in the frequency range from 10<sup>5</sup> to 10<sup>-2</sup> Hz. The scanning rate of potentiodynamic measurement is 0.166 mV/s. The scanning range of potentiodynamic measurement is from -0.3 vs.  $E_{\text{corr}}$  to +1 vs.  $E_{\text{corr}}$ , in which  $E_{\text{corr}}$  is the corrosion potential of the system.

## 2.3 Microelectrode probe

Figure 2 shows the preparation process of microelectrode probe sample for tribocorrosion test. The microelectrode probe and surrounding steel were made of the same stainless steel. The microelectrode probe was encapsulated in surrounding steel with epoxy resin. In order to avoid vacuoles generating in epoxy resin during solidification, encapsulation was processed in vacuum, as shown in Fig. 2a. Diameter of the probe is 3 mm, exposing approximate 7 mm<sup>2</sup> in corrosive liquid. In Fig. 2c, the gap

between the microelectrode probe and the surrounding steel is about 250 μm, eliminating effects caused by galvanic corrosion. Meanwhile, the small gap brings little influence on wear process of the sample.

## 2.4 Tribocorrosion measurements

Tribocorrosion measurements were performed by Rtec MFT-5000 tribometer, as shown in Fig. 3. Microelectrode samples and insulating PEEK spherical caps were constituted as friction pairs. The spherical cap with flat area of about 46 mm<sup>2</sup> could adapt automatically in ball socket of holder, to maintain flat-flat contact. The applied loads were 1, 20 and 100 N, respectively. Reciprocating frequency was 2 Hz and the single stroke is 4 mm, so that the whole exposure area of the microelectrode probe keeps contacting with the count pair during measurements. All friction pairs were submerged in 3.5% NaCl or 0.5 mol/L H<sub>2</sub>SO<sub>4</sub> solutions during the measurements.

In order to investigate the influence of the friction on corrosion behaviors, electrochemical measurements with a standard three-electrode system were performed during tribocorrosion tests. For the purpose of accurate measurements, two Pt sheets were used as a counter electrode system and two SCE electrodes were used as a reference electrode system. Before potentiodynamic measurements, pre-wear testing was carried out in solutions for 20 min, in order to get a stable potential. The scanning range of potentiodynamic measurement in tribocorrosion is from -1 vs.  $E_{\text{ref}}$  to +1 vs.  $E_{\text{ref}}$ , with the scanning rate of 0.5 mV/s, while the tests for measuring friction coefficient and wear morphologies last 30 min under same conditions but without electrochemical measurements.  $E_{\text{ref}}$  is the potential of the reference electrode.

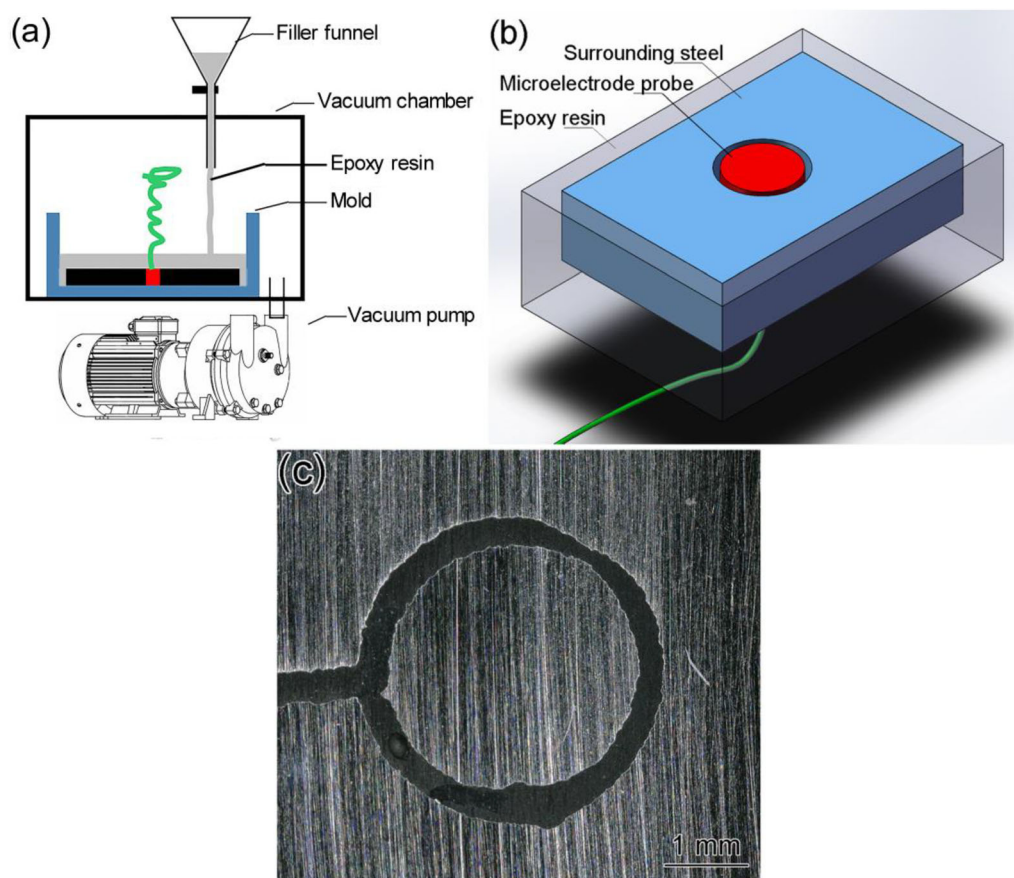


**Fig. 2** Preparation process of microelectrode probe sample. **a** Schematic diagram of vacuum encapsulation; **b** 3D-diagram of microelectrode probe sample; **c** microphotograph of microelectrode probe

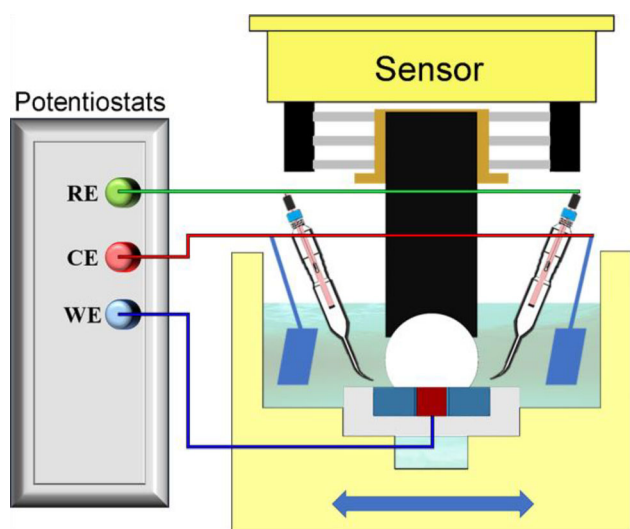


**Fig. 3** Schematic diagram of tribocorrosion measurements. RE—Reference electrode; CE—counter electrode; WE—working electrode

## 3 Results

### 3.1 Static corrosion behaviors of stainless steels

The electrochemical polarization behavior of AISI 304 and Cr26Mo1 steels in 3.5% NaCl solution is illustrated in Fig. 4.  $E_{\text{corr}}$  and an obvious passivation region are indications of a stable passive system of stainless steels and the Tafel slope is about  $b_c \approx 156$  mV/dec which means that cathodic action is dominated by oxygen reduction reaction (ORR). Both AISI 304 and Cr26Mo1 stainless steels have a small corrosion rate ( $i_{\text{corr}}$ ), less than  $2 \times 10^{-7}$  A cm<sup>-2</sup>. Comparing with AISI 304 steel, Cr26Mo1 steel has a little higher  $E_{\text{corr}}$ , a larger passivation region and a little lower corrosion rate due to its ultrapure microstructure with less inclusions, together with the influence of increasing Cr content [26]. Besides, some peaks characterized by noisy current increase can be observed on the anodic curve of AISI 304 steel, which indicates the initiation and spontaneous repassivation of many pits [27]. AISI 304 steel has an obvious breakdown potential ( $E_b$ ), due to pitting

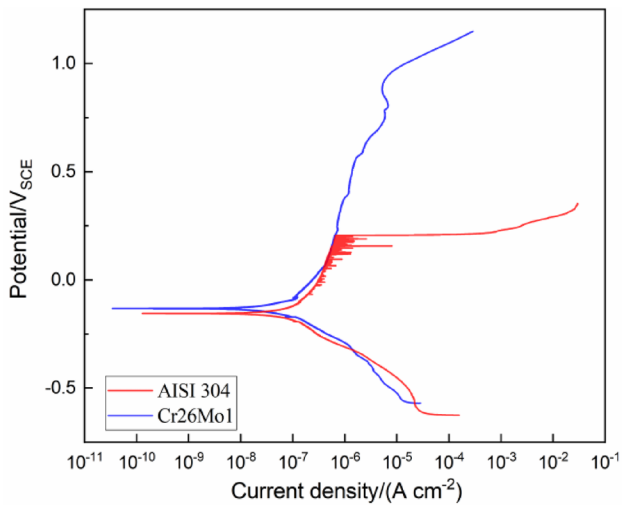


**Fig. 4** Potentiodynamic polarization curves of stainless steel in 3.5% NaCl solution

corrosion in chloride containing solutions [28], while it is not shown in the curve of Cr26Mo1 steel.

The result of EIS measurements of samples in 3.5% NaCl solution is illustrated in Fig. 5. Nyquist diagram exhibits a depressed semi-circle with a capacitive arc. In

this situation, constant phase element (CPE) is more reasonable to describe the behavior of a double layer, which is an imperfect capacitor [29]. Combined with Bode diagram, one time constant is observed. The equivalent circuit in Fig. 5d is used for fitting EIS data to quantify the electrochemical parameters [30],  $R_s$  is the solution resistance, CPE is an electrical double layer constant phase of the passive film/electrolyte interface, and  $R_t$  is a charge transfer resistance at the passive film/electrolyte interface. The parameters obtained from the fitting of EIS diagrams are shown in Table 3.  $R_s$  is the solution resistance and  $R_t$  is the transfer resistance. Both  $Y_0$  and  $n$  are constants of CPE, corresponding to modulus of the CPE admittance and dispersion coefficient, respectively. In Bode plot, the phase angles exhibit a wide peak with values of approximately  $-80^\circ$  in the frequency ranging from 1 to 100 Hz. These results indicate that the protective passive films are formed on the surface of two kinds of stainless steels in 3.5% NaCl solution, which is also proved before [31]. Both  $R_t$  and  $Y_0$  for Cr26Mo1 steel are higher than those for AISI 304 steel and it can be concluded that the passive film and the electrical double layer formed on Cr26Mo1 steel has less

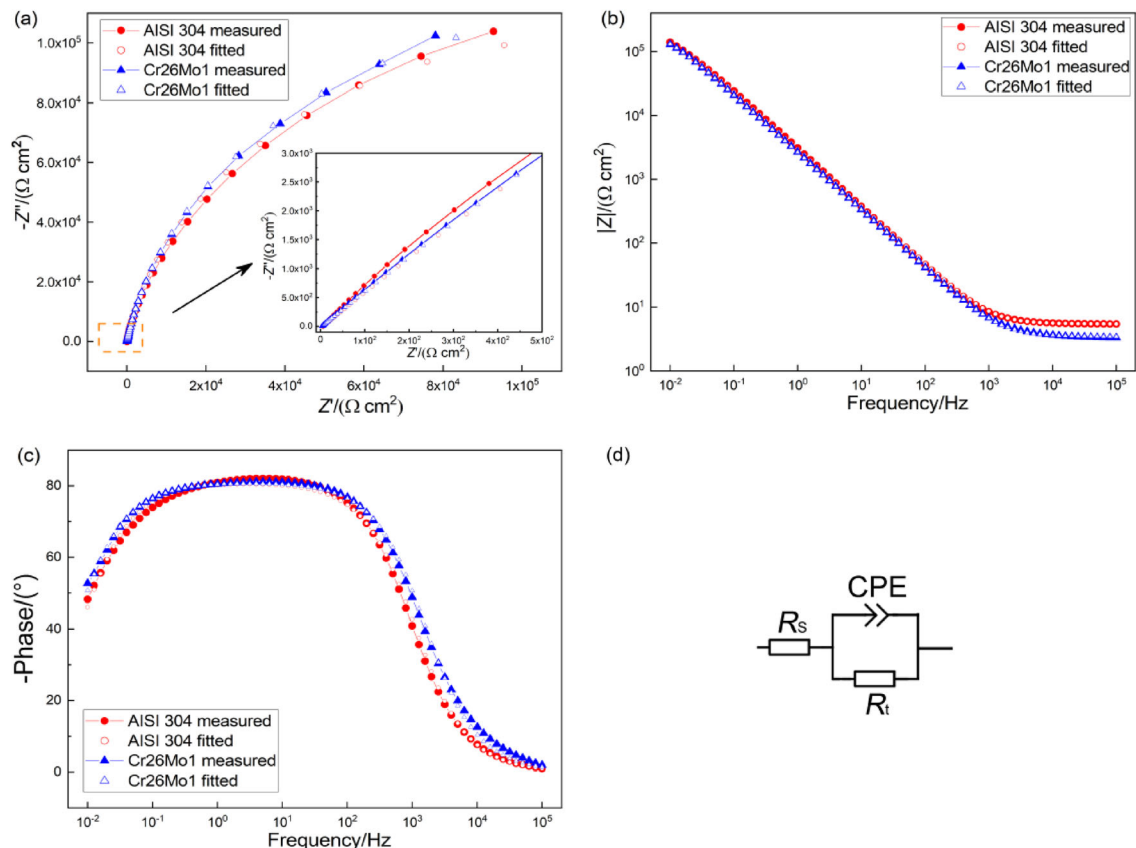


**Fig. 5** EIS measurements of stainless steels in 3.5% NaCl solution. **a** Nyquist plot; **b** Bode- $|Z|$  plot; **c** Bode-phase plot; **d** equivalent circuit.  $Z'$ —Real part of impedance;  $-Z''$ —imaginary part of impedance;  $|Z|$ —modulus of impedance

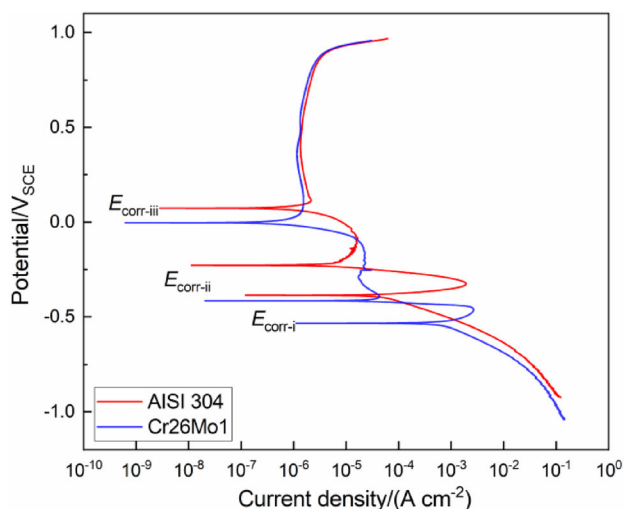
**Table 3** Electrochemical impedance parameters obtained from fitting of EIS results in 3.5% NaCl solution

Steel	$R_s/(\Omega \text{ cm}^2)$	$Y_0/(\Omega^{-1} \text{ S}^n \text{ cm}^{-2})$	$n$	$R_f/(\Omega \text{ cm}^2)$
AISI 304	5.45	$6.40 \times 10^{-5}$	0.90	$2.38 \times 10^5$
Cr26Mo1	3.45	$7.20 \times 10^{-5}$	0.90	$2.57 \times 10^5$

defects than that on AISI 304 steel, which results in a better protection effect.

The electrochemical polarization behavior of AISI 304 and Cr26Mo1 steels in 0.5 mol/L  $\text{H}_2\text{SO}_4$  solution is illustrated in Fig. 6. Three corrosion potentials are observed in Fig. 6, which stand for the active, active–passive and passive regions, respectively. Without applied potential, corrosion occurs at the lowest corrosion potential  $E_{\text{corr-i}}$ , and cathodic Tafel slope  $b_c$  is about 120 mV/dec, which means the cathodic reaction is hydrogen evolution reaction (HER).  $E_{\text{corr-i}}$  of Cr26Mo1 steel is much lower than that of AISI 304 steel. Cr26Mo1 steel is corroded at a rate of  $7.6 \times 10^{-4} \text{ A cm}^{-2}$ , which is an order of magnitude higher than that of AISI 304 steel.

From the consequence of EIS measurements in 0.5 mol/L  $\text{H}_2\text{SO}_4$  solution, especially in Nyquist diagram (Fig. 7), an inductive arc is obviously observed in quadrant IV, indicating that stainless steels dissolve in this solution. As suggested in literatures [32–34], the equivalent circuit, Fig. 7d, is used to fit EIS data. The inductive contribution is composed of the inductive resistance  $R_1$  and the inductance  $L$  connected in series [34]. The inductive arc attributed to the formation of Fe(I) or Fe(II) adsorbed intermediate species in the active region [32, 35, 36], which are responsible for the product of an adsorbed

**Fig. 6** Potentiodynamic polarization curves of stainless steel in 0.5 mol/L  $\text{H}_2\text{SO}_4$  solution

protective layer that can be considered as the precursor of a passive film [36]. The parameters obtained from the fitting of EIS diagrams are shown in Table 4. It is obvious that AISI 304 steel has a much better corrosion resistance than Cr26Mo1 steel in 0.5 mol/L  $\text{H}_2\text{SO}_4$  solution, which is consistent with the results of potentiodynamic measurements.

## 3.2 Tribocorrosion behaviors of stainless steels

### 3.2.1 Corrosion potential and corrosion rate

Referring to electrochemical polarization diagram (Fig. 8), in 3.5% NaCl solution, all of the curves shift to current increasing direction when load was applied compared to static curve (black curve). At 1 N load condition, the corrosion rate increases to more than one hundred times as origin. Meanwhile,  $E_{\text{corr}}$  is around  $-500 \text{ mV}$  versus SCE, showing that corrosion occurs in active region. At 20 N load condition,  $E_{\text{corr}}$  switches to more negative potential, while  $i_{\text{corr}}$  has little change compared with 1 N condition. As applied load increases to 100 N,  $E_{\text{corr}}$  turns to about  $-200 \text{ mV}$  versus SCE and  $i_{\text{corr}}$  decreases about one order of magnitude, compared with 1 and 20 N load. In this condition, it seems that the corrosion of stainless steels occurs in passive region. While compared with tribocorrosion in 3.5% NaCl solution, friction brings little influences on both  $E_{\text{corr-i}}$  and  $i_{\text{corr-i}}$  in 0.5 mol/L  $\text{H}_2\text{SO}_4$  solution. All of  $E_{\text{corr-i}}$  are around  $-500 \text{ mV}$  versus SCE, indicating that the surface of stainless steels maintains active state during tribocorrosion process.

Besides  $E_{\text{corr}}$  and  $i_{\text{corr}}$ , friction also affects other electrochemical parameters. Compared with static corrosion, the cathodic polarization current of stainless steels decreases obviously under friction state which decreases with the increase in applied load, especially at more negative potential. This may be related to the liquid membrane on sample surfaces. With the increase in the applied load, the thickness of the liquid membrane between the friction pair decreases; thus, the solution resistance increases and the electrochemical mass transfer process is restricted. With loading application, passive current density ( $i_p$ ) of stainless steels increases for at least half an order of magnitude compared with static situation, indicating that the passive film is damaged to a certain extent and its corrosion resistance decreases. In 3.5% NaCl solution, as applied load increases,  $i_p$  first increases and then decreases and there is little difference between AISI 304 and Cr26Mo1 steels for  $i_p$  under the same load. While in 0.5 mol/L  $\text{H}_2\text{SO}_4$  solution, as applied load increases,  $i_p$  first decreases and then increases and  $i_p$  of AISI 304 steel is a little smaller than that of Cr26Mo1 steel under the same load. The changes of  $i_p$  with applied load indicate that there

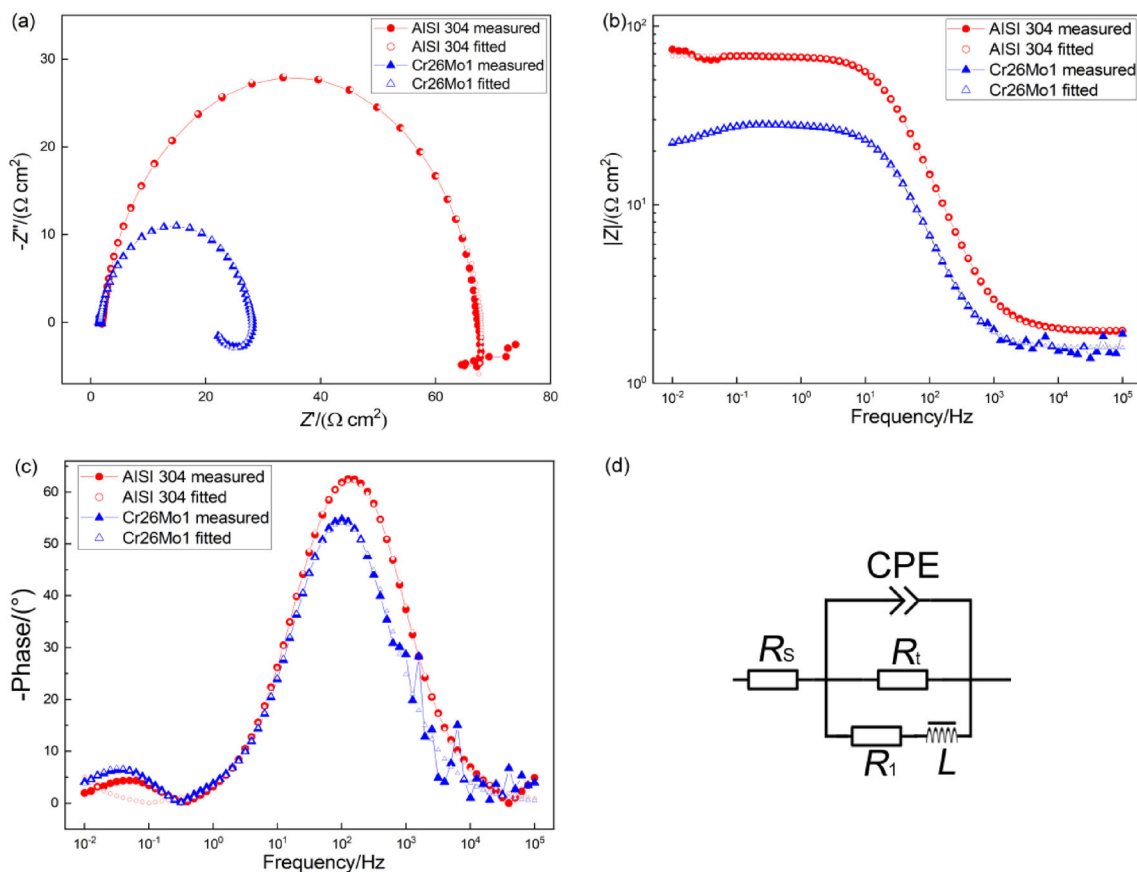


**Fig. 7** EIS measurements of stainless steels in 0.5 mol/L H<sub>2</sub>SO<sub>4</sub> solution. **a** Nyquist plot; **b** Bode-|Z| plot; **c** Bode-phase plot; **d** equivalent circuit

**Table 4** Electrochemical impedance parameters obtained from fitting of EIS results in 0.5 mol/L H<sub>2</sub>SO<sub>4</sub> solution

Steel	$R_s/(\Omega \text{ cm}^2)$	$Y_0/(\Omega^{-1} \text{ S}^n \text{ cm}^{-2})$	$n$	$R_t/(\Omega \text{ cm}^2)$	$R_1/(\Omega \text{ cm}^2)$	$L/(\text{H cm}^2)$
AISI 304	1.99	$2.07 \times 10^{-4}$	0.90	66.10	$1.89 \times 10^{-7}$	$1.15 \times 10^4$
Cr26Mo1	1.58	$5.38 \times 10^{-4}$	0.88	26.57	89.02	$4.80 \times 10^2$

is a competitive mechanism for passive film during tribo-corrosion. Additionally, friction raises the breakdown potential ( $E_{bd}$ ) of AISI 304 and reduces the tendency of pitting corrosion.

All of  $i_{corr}$ ,  $E_{corr}$  and  $i_p$  are listed in Tables 5 and 6.

**3.2.2 Wear morphologies and friction coefficient**

Figures 9 and 10 show surface morphologies of wear track of stainless steels under different applied loads after tribocorrosion tests in 3.5% NaCl solution. Under 1 and 20 N applied load conditions, the surface is damaged and mainly appears scratches and furrows. Under 100 N condition, morphologies are obviously different, in which pieces of wear debris and corrosion productions can be observed on the surface of wear tracks. For further analysis, Raman

analysis (wavelength of 532 nm) for wear scar in Fig. 10d was performed to identify the compositions of surface layer, as shown in Fig. 11. It indicates that apart from PEEK transfer debris [37], the surface layer consists of mainly Cr<sub>2</sub>O<sub>3</sub>, FeCr<sub>2</sub>O<sub>4</sub>,  $\gamma$ -Fe<sub>2</sub>O<sub>3</sub>,  $\beta$ -FeOOH and Fe<sub>3</sub>O<sub>4</sub> [38–40]. Thus, the wear track was covered by an oxide film with cracks due to the effect of cyclic grinding and electrochemical reaction. Compared with Cr26Mo1 steel, there are some craterlets on AISI 304 steel surface, deriving from pit corrosion.

Surface morphologies of wear track of stainless steels under different applied loads after tribocorrosion tests in 0.5 mol/L H<sub>2</sub>SO<sub>4</sub> solution are illustrated in Figs. 12 and 13. Stainless steels show intact surface after static immersing for 30 min without friction. However, the joining of friction remodels the morphologies obviously. Serried furrows

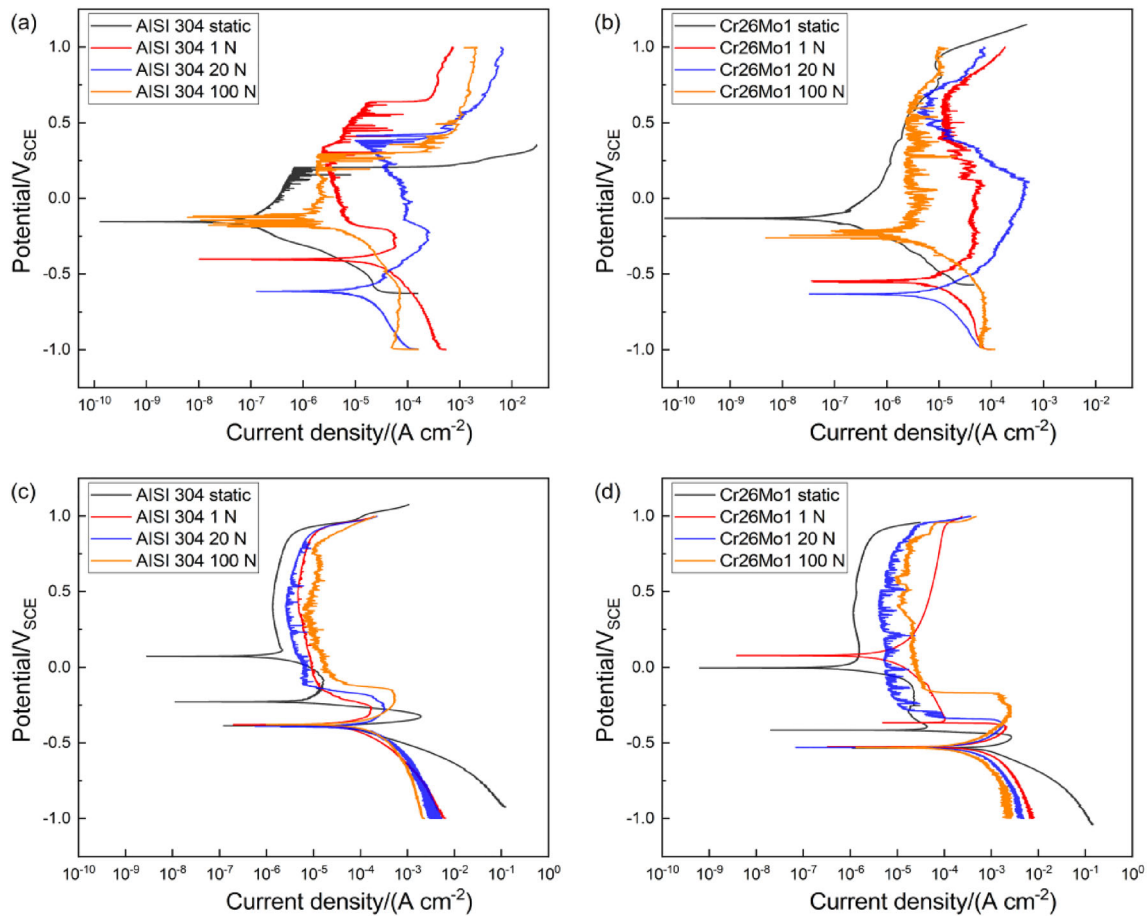


**Fig. 8** Tribocorrosion potentiodynamic polarization curves of AISI 304 (a, c) and Cr26Mo1 (b, d) steels in 3.5% NaCl solution (a, b) and 0.5 mol/L H<sub>2</sub>SO<sub>4</sub> solution (c, d)

**Table 5**  $E_{\text{corr}}$  and  $i_{\text{corr}}$  of stainless steels in 3.5% NaCl solution

Applied load/N	AISI 304 steel			Cr26Mo1 steel		
	$E_{\text{corr}}/V_{\text{SCE}}$	$i_{\text{corr}}/(A\text{ cm}^{-2})$	$i_p/(A\text{ cm}^{-2})$	$E_{\text{corr}}/V_{\text{SCE}}$	$i_{\text{corr}}/(A\text{ cm}^{-2})$	$i_p/(A\text{ cm}^{-2})$
No friction	-0.15	$1.6 \times 10^{-7}$	$6.4 \times 10^{-7}$	-0.13	$1.3 \times 10^{-7}$	$5.8 \times 10^{-7}$
1	-0.40	$2.3 \times 10^{-5}$	$3.4 \times 10^{-6}$	-0.55	$8.3 \times 10^{-6}$	$1.5 \times 10^{-5}$
20	-0.61	$1.2 \times 10^{-5}$	$1.7 \times 10^{-5}$	-0.63	$7.2 \times 10^{-6}$	$6.6 \times 10^{-6}$
100	-0.15	$1.2 \times 10^{-6}$	$2.3 \times 10^{-6}$	-0.26	$3.1 \times 10^{-6}$	$3.3 \times 10^{-6}$

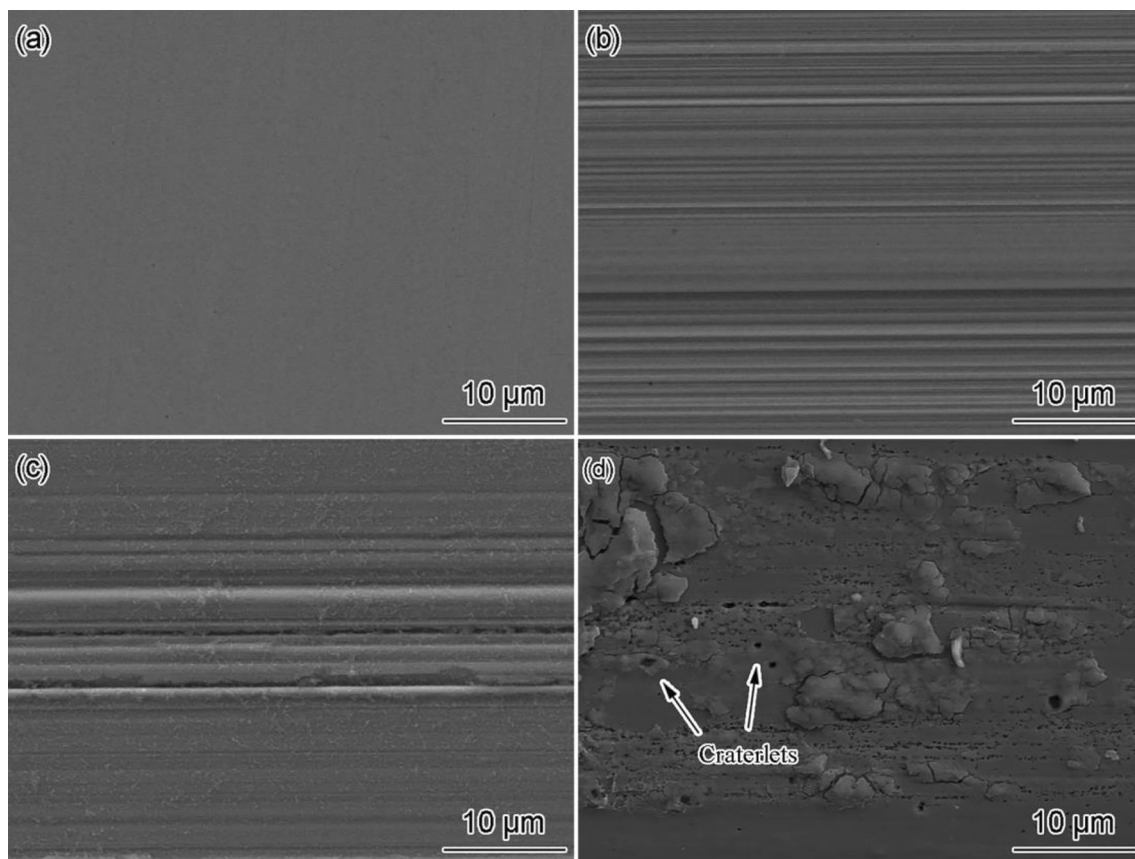
can be found on the wear scar, together with the character of brittle spalling, due to the influence of corrosive medium on the surface [41, 42]. With applied load increasing, the furrows of Cr26Mo1 steel become much denser, but for AISI 304 steel, the reverse is true. The surface morphology of AISI 304 steel under 100 N condition is much smoother than that under low applied load, similar to be polished. From Fig. 12e, f, no oxygen was detected on the wear track surface even when the applied load increased to 100 N,

which means that no oxide film formed on the surface of wear track.

Friction coefficient can reflect the status of friction and lower friction coefficient represents smoother friction interface and less energy consumed in the friction process. Figure 14 shows that friction coefficient of stainless steels in 3.5% NaCl solution is much smaller than that in 0.5 mol/L H<sub>2</sub>SO<sub>4</sub> solution. The friction coefficients of the two steels are similar in 3.5% NaCl solution, while in 0.5 mol/L H<sub>2</sub>SO<sub>4</sub> solution, the friction coefficients of Cr26Mo1 steel

**Table 6**  $E_{\text{corr}}$  and  $i_{\text{corr}}$  of stainless steels in 0.5 mol/L  $\text{H}_2\text{SO}_4$  solution

Applied load/N	AISI 304 steel			Cr26Mo1 steel		
	$E_{\text{corr}-i}/V_{\text{SCE}}$	$i_{\text{corr}-i}/(\text{A cm}^{-2})$	$i_p/(\text{A cm}^{-2})$	$E_{\text{corr}-i}/V_{\text{SCE}}$	$i_{\text{corr}-i}/(\text{A cm}^{-2})$	$i_p/(\text{A cm}^{-2})$
No friction	-0.39	$4.7 \times 10^{-5}$	$1.5 \times 10^{-6}$	-0.53	$7.1 \times 10^{-4}$	$1.3 \times 10^{-6}$
1	-0.38	$5.6 \times 10^{-5}$	$5.4 \times 10^{-6}$	-0.52	$8.4 \times 10^{-4}$	$6.9 \times 10^{-5}$
20	-0.39	$1.2 \times 10^{-4}$	$3.1 \times 10^{-6}$	-0.53	$6.2 \times 10^{-4}$	$5.7 \times 10^{-6}$
100	-0.38	$1.4 \times 10^{-4}$	$9.7 \times 10^{-6}$	-0.53	$4.3 \times 10^{-4}$	$1.7 \times 10^{-5}$

**Fig. 9** Morphologies of AISI 304 after tribocorrosion for 30 min in 3.5% NaCl. **a** No friction; **b** 1 N; **c** 20 N; **d** 100 N

are much higher than those of AISI 304 steel. These are corresponding to morphologies analyses. The wear surface of stainless steels in 0.5 mol/L  $\text{H}_2\text{SO}_4$  is rougher than that in 3.5% NaCl solution. In 0.5 mol/L  $\text{H}_2\text{SO}_4$  solution, the wear surface of AISI 304 steel is smoother than that of Cr26Mo1 steel. With applied load increasing, the friction coefficient of stainless steels shows a decreasing trend in the two solutions except AISI 304 steel with 1 N in 0.5 mol/L  $\text{H}_2\text{SO}_4$ . However, it decreased obviously in 3.5% NaCl solution especially under 100 N load, which is related to oxide film on the wear track and PEEK transferred from the count pair [43].

## 4 Discussion

### 4.1 Effects of alloying elements, mechanical properties of stainless steels and test media on tribocorrosion behaviors

As a significant alloying element, the content of Cr affects corrosion behaviors of stainless steels. As Cr content increases, it enlarges the passive region of stainless steels and makes active anodic curve shift to negative potential [44], due to its more negative standard electrode potential.

In self-passivation medium, ORR dominates cathodic reaction and corrosion occurs in passive region at more

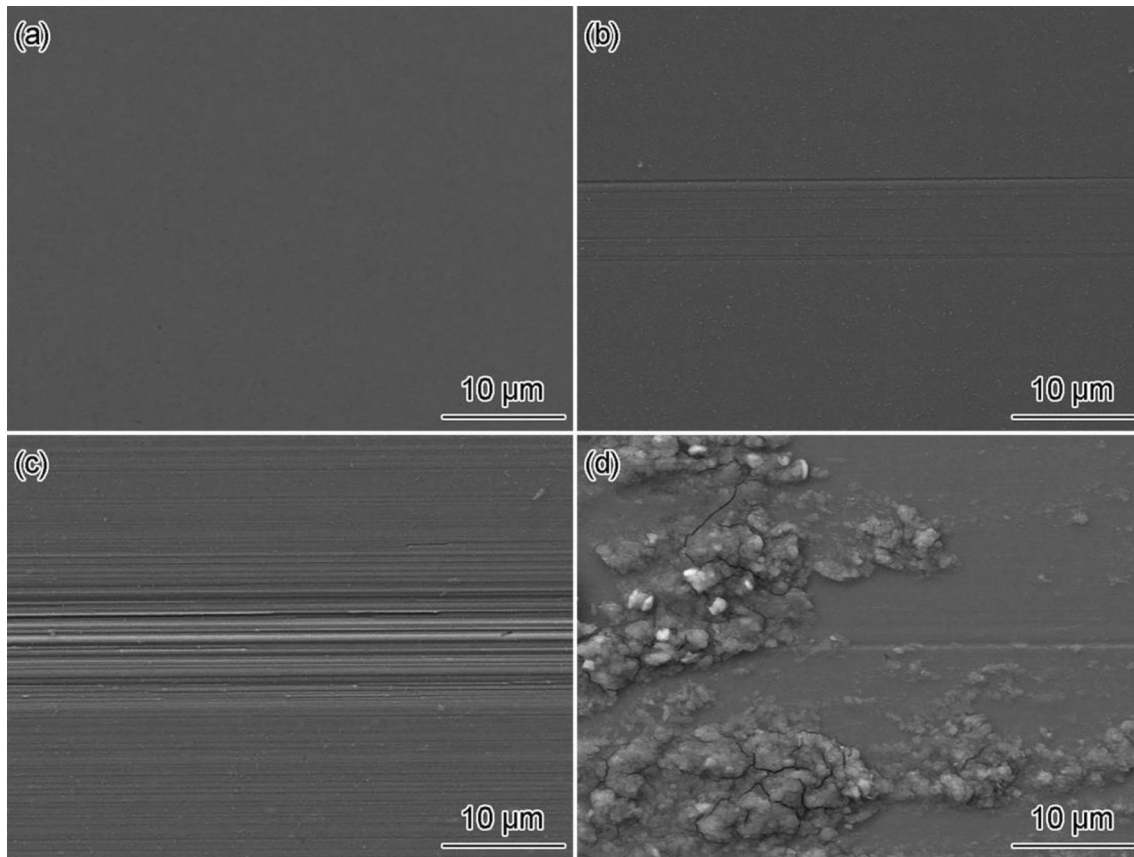


**Fig. 10** Morphologies of Cr26Mo1 after tribocorrosion for 30 min in 3.5% NaCl. **a** No friction; **b** 1 N; **c** 20 N; **d** 100 N

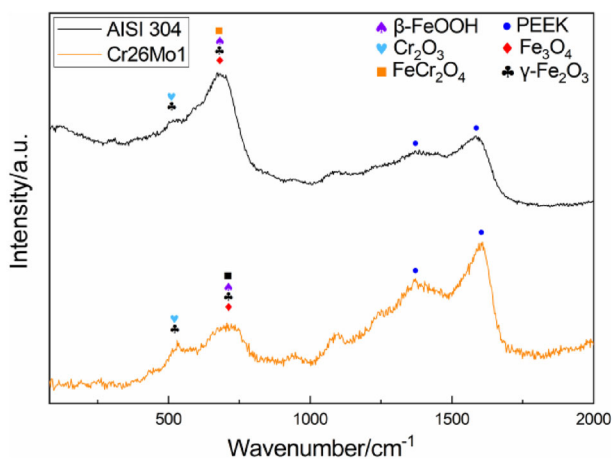


**Fig. 11** Raman spectra of tribocorrosion production in 3.5% NaCl under 100 N load

positive potential. In 3.5% NaCl solution, two kinds of stainless steels perform similarly and passive film can form on the surface. The high Cr content of Cr26Mo1 steel has a little effect on corrosion rate in 3.5% NaCl solution compared with AISI 304 steel, reflected in more positive  $E_{\text{corr}}$ , smaller corrosion rate and higher impedance of passive film. Furthermore, Cr26Mo1 steel has a larger passivation

region and less tendency of pitting corrosion corresponds with electrochemical polarization behavior, which attribute to high Cr content [45–47]. While in reducibility medium, HER cathodic reaction makes corrosion occur in active region at more negative potential. In 0.5 mol/L  $\text{H}_2\text{SO}_4$  solution, with such high hydron concentration, the restriction of passive reaction results in no protective passive films forming on the surface and stainless steels dissolving. Higher Cr content makes Cr26Mo1 steel get corroded at more negative potential with larger corrosion rate. Thus, the corrosion mechanism diagram of stainless steels can be described in Fig. 15. Combining with Butler–Volmer equation, the difference of corrosion potential between AISI 304 and Cr26Mo1 steels,  $\Delta E_{\text{corr-i}}$ , can be calculated by Eq. (1).

$$\Delta E_{\text{corr-i}} = E_{\text{AISI304corr-i}} - E_{\text{Cr26Mo1corr-i}} = -\frac{2.303RT}{\alpha nF} (\lg i_{\text{AISI304corr-i}} - \lg i_{\text{Cr26Mo1corr-i}}) \quad (1)$$

where  $E_{\text{AISI304corr-i}}$  and  $i_{\text{AISI304corr-i}}$  are the lowest corrosion potential and corrosion current density of 304 stainless steel, respectively; and  $E_{\text{Cr26Mo1corr-i}}$  and  $i_{\text{Cr26Mo1corr-i}}$  are the lowest corrosion potential and corrosion current density of Cr26Mo1 stainless steel, respectively.

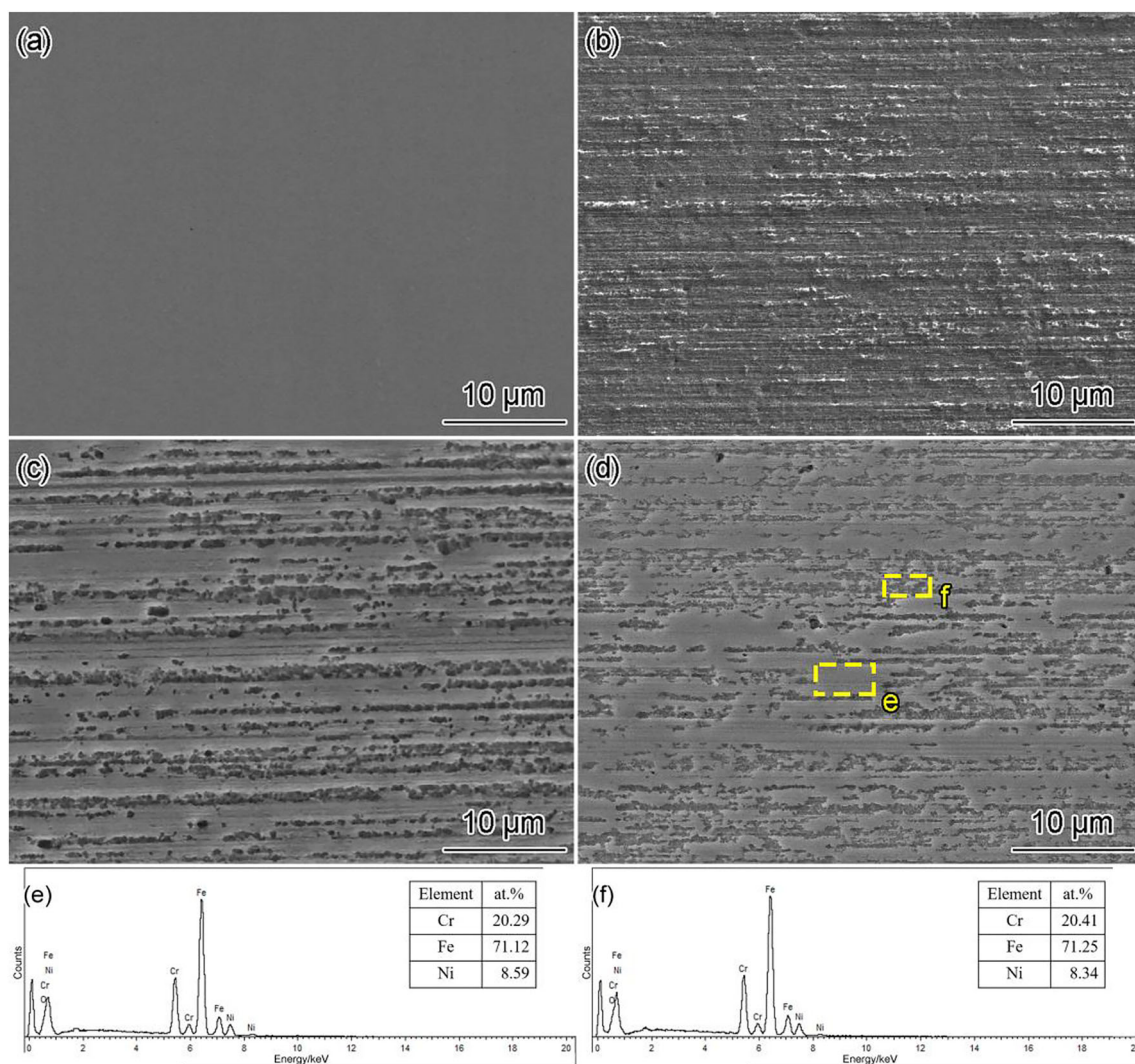


**Fig. 12** Morphologies (a–d) and EDS (e, f) of AISI 304 steel after tribocorrosion for 30 min in 0.5 mol/L H<sub>2</sub>SO<sub>4</sub>. **a** No friction; **b** 1 N; **c** 20 N; **d** 100 N; **e** area e in **d**; **f** area f in **d**

As  $b_c = 2.303RT/(nF) = 120$  mV/dec,  $i_{\text{AISI304corr-i}} = 4.7 \times 10^{-5}$  A cm<sup>-2</sup>,  $i_{\text{Cr26Mo1corr-i}} = 7.1 \times 10^{-4}$  A cm<sup>-2</sup>, the calculated result  $\Delta E_{\text{corr-i}} = 141.5$  mV is similar to the test result (140 mV). This indicates that content of Cr is important factor on corrosion potential and thus has big influence on corrosion behavior of the steels. Therefore, high Cr content is beneficial for corrosion resistance when cathodic reaction is dominated by ORR, while harmful in HER dominated condition.

Meanwhile, Mo is very beneficial for the pitting resistance of stainless steel in aggressive Cl<sup>-</sup> ions media. According to equation for pitting resistance equivalent number (PREN), Mo has more than triple effects for enhancing PREN than Cr [1]. In 3.5% NaCl solution, Cr26Mo1 steel shows better tribocorrosion resistance with no pitting corrosion morphology in the wear track. The

addition of Mo can render the passive film more stable against breakdown in solution with Cl<sup>-</sup> [2, 3]. The erasure of Mo compounds by friction nullifies the advantage of Mo, although in acidic solutions, the formation of Mo insoluble oxides, oxyhydroxide or molybdates, enhancing the corrosion resistance [4, 5]. Ni is another important element generally providing satisfying positive effect on the acidic solution by promoting austenitizing. Although AISI 304 steel has about ten times C content than Cr26Mo1 steel, the tribocorrosion morphology of AISI 304 steel different does not show amounts of craterlets.

On one side, it can be concluded that tribocorrosion resistance mainly relies on corrosion behavior of stainless steel. Because of the smaller corrosion rate of tribocorrosion in 3.5% NaCl solution, Cr26Mo1 steel with superb resistance to pitting corrosion seems to have better

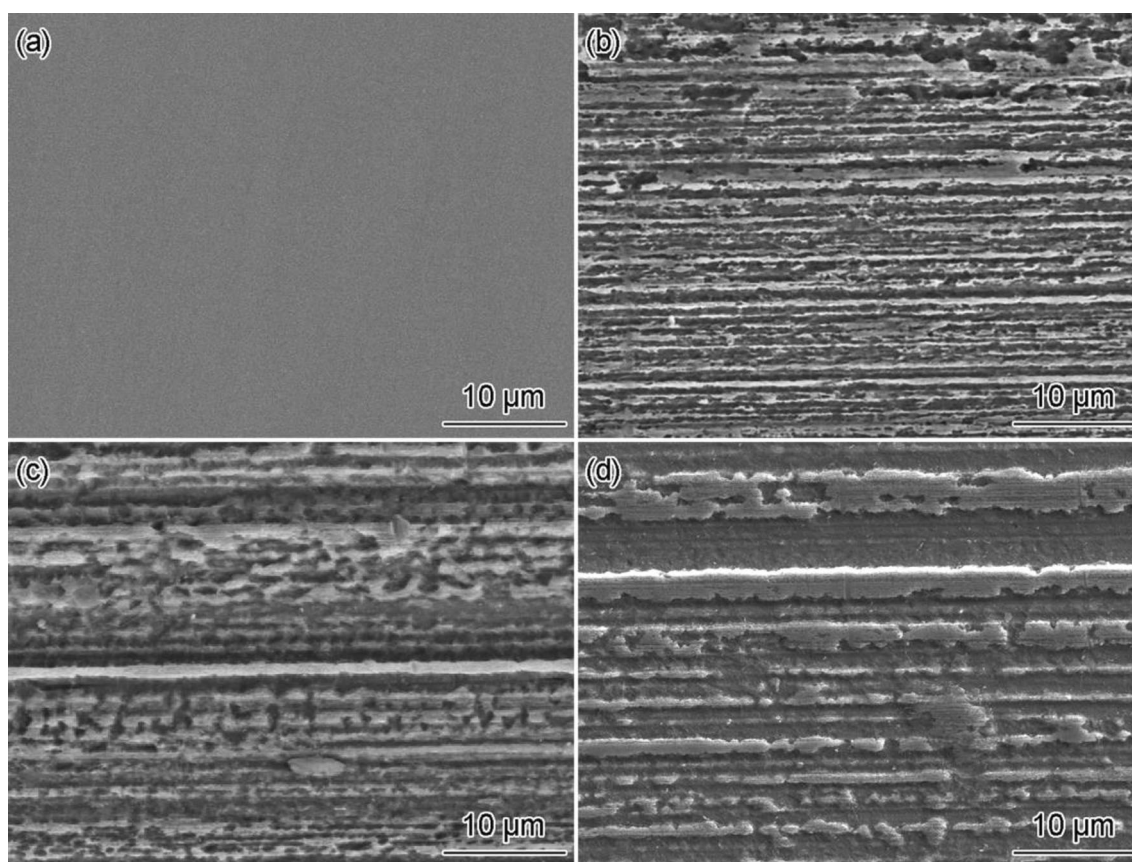


**Fig. 13** Morphologies of Cr26Mo1 steel after tribocorrosion for 30 min in 0.5 mol/L  $\text{H}_2\text{SO}_4$ . **a** No friction; **b** 1 N; **c** 20 N; **d** 100 N

tribocorrosion resistance. While in 0.5 mol/L  $\text{H}_2\text{SO}_4$  solution, smaller corrosion rate both in static corrosion and tribocorrosion makes AISI 304 has better performance.

On the other side, the effect of mechanical properties on tribocorrosion cannot be ignored. Hardness and module are significant factors on wear, which are used to evaluate plastic and elastic deformation, respectively. In some ways, high hardness and module make it difficult for materials deformation, which is beneficial for wear resistance [48, 49]. What's more, deformation can increase dislocation density which goes against corrosion performances [50, 51]. As listed in Table 2, Cr26Mo1 steel has better mechanical properties than AISI 304 steel. In 3.5% NaCl solution, the average corrosion current density of Cr26Mo1 steel under three loads is  $6.2 \times 10^{-6} \text{ A cm}^{-2}$ , which is about 48 times its static corrosion rate; the average corrosion current density of AISI 304 steel under three loads is  $1.2 \times 10^{-5} \text{ A cm}^{-2}$ , which is 75 times its static corrosion rate. In 0.5 mol/L  $\text{H}_2\text{SO}_4$  solution; the average corrosion current density of Cr26Mo1 steel under three loads is  $6.3 \times 10^{-4} \text{ A cm}^{-2}$ , which is 0.9 times as its static corrosion rate; the average corrosion current density of AISI 304 steel under three loads is  $1.1 \times 10^{-4} \text{ A cm}^{-2}$ , which is 2.3 times its static corrosion rate. In summary, in the two

solutions, the increase degree of corrosion rate for AISI 304 steel is higher than that for Cr26Mo1 steel, indicating that better mechanical properties of stainless steels are beneficial to its tribocorrosion performance.

#### 4.2 Effects of corrosive mediums on tribocorrosion behaviors of stainless steels

It is well known that corrosive mediums play important role on corrosion and tribocorrosion behavior of stainless steels. Without friction, nanoscale passive films form spontaneously and rapidly on the surface of stainless steels in 3.5% NaCl solution [52]. Once tiny damages occur on passive films, the fresh substrates expose to the corrosive medium and passive films can form on the fresh substrates immediately, namely regeneration of passive film. During friction process, the passive film on the surface of stainless steel could be wiped off by friction force and regenerated due to electrochemical reaction. Thus, the passive film undergoes a process of continuous removal and regeneration. When the removal rate is higher than regeneration rate, the fresh substrate exposes to corrosive media, which makes stainless steel exist in active dissolution state. In this

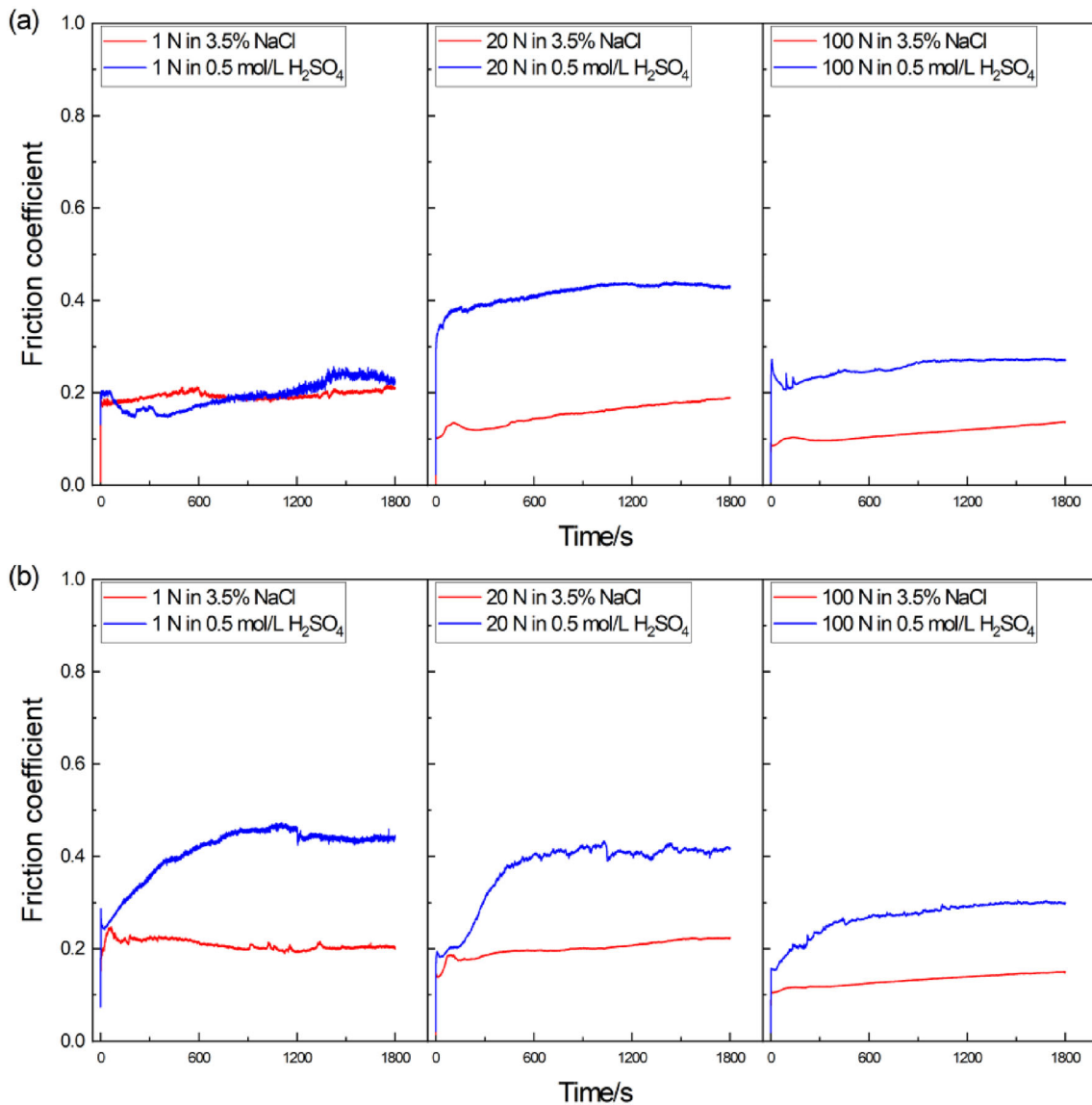


**Fig. 14** Friction coefficient of AISI 304 (a) and Cr26Mo1 (b) steels in tribocorrosion measurement

situation, friction could significantly promote corrosion. For example, in 3.5% NaCl solution, corrosion rate of stainless steels under the condition of 1 N is about 100 times that under static corrosion.

However, in 0.5 mol/L  $H_2SO_4$  solution, corrosion rate of stainless steels under the condition of 1 N is about 1.2 times static corrosion rate. It means that in 0.5 mol/L  $H_2SO_4$  solution, friction could slightly promote corrosion due to stainless steels being in active dissolution state even without friction. Compared Figs. 9 and 10 with Figs. 12 and 13, corrosive mediums show big effect on surface morphologies of the stainless steels after tribocorrosion test. Although the wear mechanism of stainless steels in both solutions is abrasive wear, plastic removal mechanism is dominant in 3.5% NaCl solution. Plastic and brittle

removal mechanisms control together in 0.5 mol/L  $H_2SO_4$  solution, resulting from hydrogen embrittlement phenomena of stainless steel. From Fig. 16, it can be seen that there are many peeling pits and cracks on the wear track, which increases the area of exposure to corrosive mediums and thus improve chemical activity of stainless steels. This kind of surface morphology could improve the active dissolution of stainless steel to a certain extent.

### 4.3 Effects of applied load on tribocorrosion of stainless steels

The ratio of  $i_{\text{corr-tribocorrosion}}$  to  $i_{\text{corr-static}}$  is shown in Fig. 17. It can be seen that the ratios of two stainless steels decrease sharply with the load increasing in 3.5% NaCl solution. In

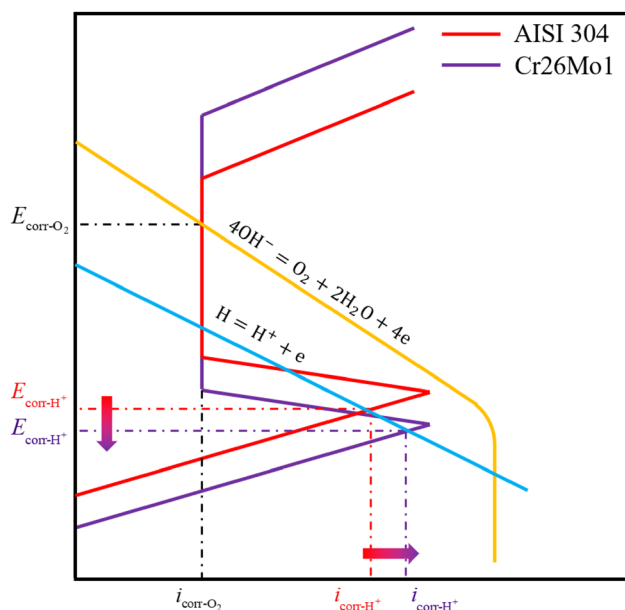


Fig. 15 Corrosion mechanism diagram of different stainless steels

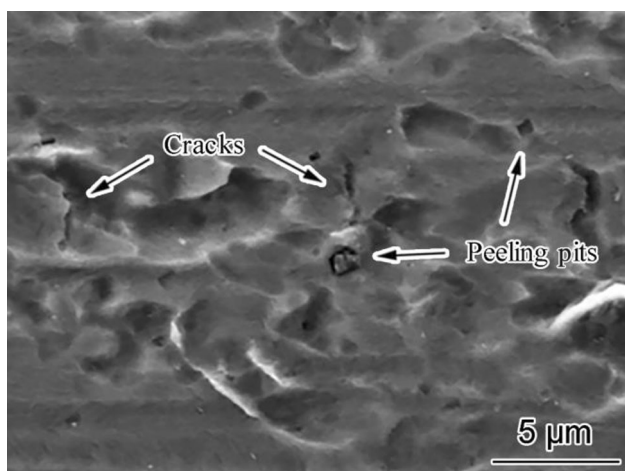


Fig. 16 Microstructures of Cr26Mo1 after 100 N tribocorrosion for 30 min in 0.5 mol/L H<sub>2</sub>SO<sub>4</sub>

0.5 mol/L H<sub>2</sub>SO<sub>4</sub> solution, the ratio does not change monotonically as the load increases for AISI 304 steel, but it still decreases for Cr26Mo1 steel. Although the ratio increases with the increase in load for AISI 304 steel, the increasing trend becomes slow above 20 N. Generally speaking, the corrosion rate of stainless steel shows a decreasing trend with the increase in the load.

In the process of friction, the surface of stainless steel may form an oxide film under the action of friction heat and normal load squeezing [53], which is called friction oxidation film. With the increase in load, the tendency of forming friction oxide film becomes stronger and stronger. In 3.5% NaCl solution, the surface of stainless steels undergoes removal and regeneration of passive film under

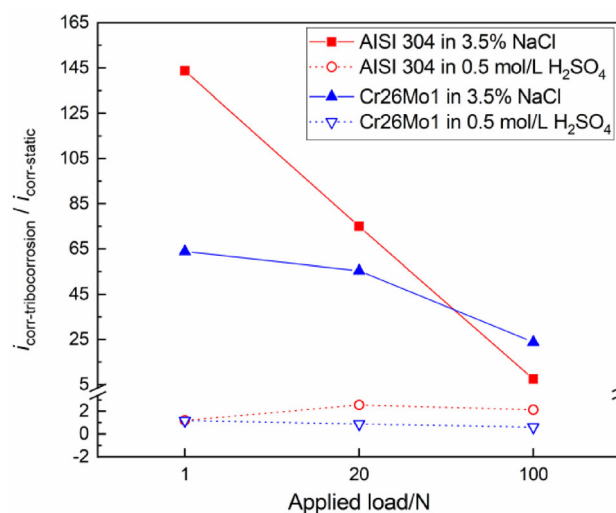
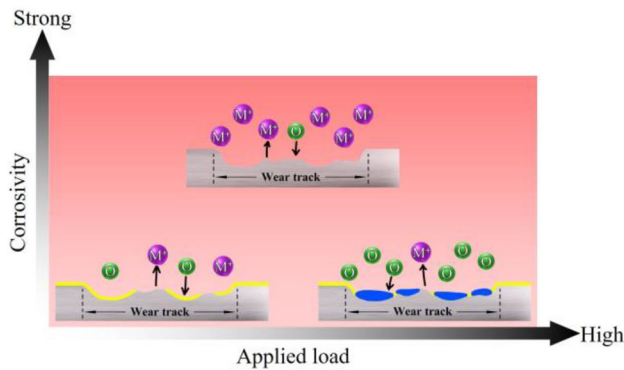


Fig. 17 Ratio of  $i_{\text{corr-tribocorrosion}}$  to  $i_{\text{corr-static}}$

low loadings. This will be replaced by the formation and excoriation processes of the friction oxide film with loading increasing. When the formation rate is greater than the excoriation rate, a stable friction oxide film will be formed on the surface of stainless steel, e.g., in the 100 N case. The friction oxide film could raise  $E_{\text{corr}}$  and decrease  $i_{\text{corr}}$ . With the thickness increase in the friction oxidation film, it may be peeled off by friction force.

With such high hydron concentration in 0.5 mol/L H<sub>2</sub>SO<sub>4</sub> solution, oxide reaction is restrained and stainless steels exist at a state of active dissolution and no passive film forms on the surface, so that during friction process, the surface of stainless steels experiences the formation of friction oxidation and the oxidation film being dissolved. Compared the two solutions, H<sup>+</sup> has strong dissolving ability, so that friction oxidation film has a high dissolution rate and it is difficult to be formed stably. Although the dissolution rate of friction oxidation film is always greater than its formation rate and the stainless steels keep active dissolution state, the formation tendency of friction oxide film could decrease corrosion rate, e.g., in 100 N case of Cr26Mo1 steel. Compared with AISI 304 steel, Cr26Mo1 steel has a stronger tendency to form friction oxide film due to its high Cr content, and its corrosion rate decreases with load increasing.

Therefore, applied load is an important factor on tribo-corrosion behaviors of stainless steels. It can be found that a certain load exists which can result in the largest corrosion rate and promote corrosion process extremely under this applied loading condition. For Cr26Mo1 steel, a small load could bring a large increase in corrosion rate. For AISI 304 steel, a small load could accelerate its corrosion process in 3.5% NaCl solution, while a high load could induce more serious corrosion in 0.5 mol/L H<sub>2</sub>SO<sub>4</sub> solution.



**Fig. 18** Schematic diagram of stainless steels surface statue changes with applied load and corrosivity

Figure 18 shows the relationship between the surface status of stainless steels and the experimental parameters (corrosive mediums, loading) when rubbed with PEEK. With applied loading increasing, the surface statue reveals the trend of forming friction oxidation film and the trend of dissolving passive film or friction oxidation film with corrosivity increasing.

## 5 Conclusions

1. In 3.5% NaCl solution, Cr26Mo1 steel shows better corrosion resistance than AISI 304 steel. While in 0.5 mol/L H<sub>2</sub>SO<sub>4</sub> solution, the consequence goes to be the opposite. The tribocorrosion behavior of stainless steels is mainly dominated by its static corrosion behaviors.
2. High Cr content and presence of Mo in stainless steels are beneficial to corrosion resistance in neutral solutions in which it can maintain passive state. While in strongly corrosive mediums, stainless steels show active state even with the high Cr content and Mo. Ni can enhance corrosion resistance of AISI 304 steel in acid solution for it can stabilize austenite. Meanwhile, better mechanical properties are in favor of tribocorrosion resistance.
3. Corrosive mediums take great impact on tribocorrosion behaviors of stainless steels, both tribocorrosion rate and morphologies. In slight corrosive mediums, friction strongly promotes corrosion reaction, but it shows the influence to a certain extent in strong corrosive mediums. The wear mechanisms of stainless steels show plastic removal in 3.5% NaCl solution and plastic and fragile removal in 0.5 mol/L H<sub>2</sub>SO<sub>4</sub> solution.
4. Applied load is an important factor in tribocorrosion behaviors of stainless steels. With the increase in applied load, the effect of friction turns into promoting

formation of the friction oxide film instead of removing passive film. What's more, a certain load exists at which corrosion process can be promoted extremely.

**Acknowledgements** The work in this paper was supported by Petro-China Key Core Technology Project (21ZG10). The work was also supported by the Strategic Priority Research Program of the Chinese Academy of Sciences (Grant No. XDC04040400).

## Declarations

**Conflict of interest** The authors declared that they have no conflicts of interest to this work.

## References

- [1] F. Majdič, J. Pezdirnik, M. Kalin, *Tribol. Int.* 44 (2011) 2013–2021.
- [2] Y. Ding, R. Liu, J. Yao, Q. Zhang, L. Wang, *Surf. Coat. Technol.* 329 (2017) 97–108.
- [3] M. Fazel, H.R. Salimijazi, M.A. Golozar, M.R. Garsivaz jazi, *Appl. Surf. Sci.* 324 (2015) 751–756.
- [4] B. Hou, X. Li, X. Ma, C. Du, D. Zhang, M. Zheng, W. Xu, D. Lu, F. Ma, *npj Mater. Degrad.* 1 (2017) 1–10.
- [5] M.S.D. Coseglio, *Mater. Sci. Technol.* 33 (2017) 1863–1878.
- [6] M. Liu, D.L. Duan, S.L. Jiang, M.Y. Li, S. Li, *Acta Metall. Sin. (Engl. Lett.)* 31 (2018) 1049–1058.
- [7] Y. Sun, V. Rana, *Mater. Chem. Phys.* 129 (2011) 138–147.
- [8] S. Mischler, S. Debaud, D. Landolt, *J. Electrochem. Soc.* 145 (1998) 750–758.
- [9] M. Azzi, M. Paquette, J.A. Szpunar, J.E. Klemberg-Sapieha, L. Martinu, *Wear* 267 (2009) 860–866.
- [10] N. Diomidis, J.P. Celis, P. Ponthiaux, F. Wenger, *Wear* 269 (2010) 93–103.
- [11] F. Bartolomeu, M. Buciumeanu, E. Pinto, N. Alves, O. Carvalho, F.S. Silva, G. Miranda, *Addit. Manuf.* 16 (2017) 81–89.
- [12] Z. Dai, M. Liu, S. Jiang, M. Li, S. Li, D. Duan, *J. Mater. Eng. Perform.* 31 (2022) 2708–2714.
- [13] J. Geringer, B. Forest, P. Combrade, *Wear* 261 (2006) 971–979.
- [14] A. Golchin, G.F. Simmons, S. Glavatskih, B. Prakash, *Proc. Inst. Mech. Eng. Part J.* 227 (2013) 811–825.
- [15] J.C. M. Souza, A.C. Bentes, K. Reis, S. Gavinha, M. Buciumeanu, B. Henriques, F.S. Silva, J. R. Gomes, *Tribol. Int.* 102 (2016) 154–160.
- [16] F.L. Yin, X. Zhou, S.L. Nie, H. Ji, Z. Hu, *Int. J. Electrochem. Sci.* 14 (2019) 4643–4658.
- [17] S. Mischler, in: 3rd International Symposium on Tribo-Corrosion Atlanta, GA, USA, 2012, pp. 1–18.
- [18] S. Mischler, *Tribol. Int.* 41 (2008) 573–583.
- [19] A.C. Vieira, L.A. Rocha, N. Papageorgiou, S. Mischler, *Corros. Sci.* 54 (2012) 26–35.
- [20] D. Landolt, S. Mischler, M. Stemp, *Electrochim. Acta* 46 (2001) 3913–3929.
- [21] A. Stachowiak, W. Zwierycki, *Tribol. Int.* 44 (2011) 1216–1224.
- [22] D.B. Harrison, D.M. Nicholas, G.M. Evans, *J. Am. Water Works Assoc.* 96 (2004) 67–76.
- [23] X. Wei, J.H. Dong, J. Tong, Z. Zheng, W. Ke, *Acta Metall. Sin.* 48 (2012) 502–507.
- [24] X. Wei, J.H. Dong, J. Tong, Z. Zheng, W. Ke, *Int. J. Electrochem. Sci.* 8 (2013) 887–902.

- [25] Y.Y. Zhu, L.K. Ning, T.Z. Xin, E.Z. Liu, J. Tong, Z. Tan, Y.T. Zhou, Z. Zheng, *J. Iron Steel Res. Int.* 28 (2021) 1291–1304.
- [26] X.M. Zhu, Y.S. Zhang, *Corrosion* 54 (1998) 3–12.
- [27] N.J. Laycock, *Corrosion* 55 (1999) 590–595.
- [28] Z. Szklarska-Smialowska, *Pitting corrosion of metals*, National Association of Corrosion Engineers, Houston, Texas, USA, 1986.
- [29] F. Mohammadi, T. Nickchi, M.M. Attar, A. Alfantazi, *Electrochim. Acta* 56 (2011) 8727–8733.
- [30] Y.X. Qiao, D.K. Xu, S. Wang, Y.J. Ma, J. Chen, Y.X. Wang, H.L. Zhou, *Metals* 9 (2019) 1213.
- [31] C.N. Cao, J.Q. Zhang, *An introduction to electrochemical impedance spectroscopy*, Science, Beijing, China, 2002.
- [32] A. Pardo, M.C. Merino, A.E. Coy, F. Viejo, R. Arrabal, E. Matykina, *Corros. Sci.* 50 (2008) 780–794.
- [33] M. Orazem, B. Tribollet, *Electrochemical impedance spectroscopy*, John Wiley & Sons, Inc., Hoboken, NJ, USA, 2008.
- [34] A. Pardo, M. C. Merino, M. Carboneras, F. Viejo, R. Arrabal, J. Muñoz, *Corros. Sci.* 48 (2006) 1075–1092.
- [35] M. Keddad, O.R. Mattos, H. Takenouti, *Electrochim. Acta* 31 (1986) 1147–1158.
- [36] T. Bellezze, G. Giuliani, A. Viceré, G. Roventi, *Corros. Sci.* 130 (2018) 12–21.
- [37] B.H. Stuart, B.J. Briscoe, *Spectrochimica Acta Part A-Molecular and Biomolecular Spectroscopy* 50 (1994) 2005–2009.
- [38] C.F. Dong, H. Luo, K. Xiao, Y. Ding, P.H. Li, X.G. Li, *Anal. Lett.* 46 (2013) 142–155.
- [39] J. Zuo, C.Y. Xu, B.H. Hou, C.S. Wang, Y. Xie, Y.T. Qian, *J. Raman Spectrosc.* 27 (1996) 921–923.
- [40] S. Inoue, H. Uchida, M. Morii, K. Koterazawa, *J. Jpn. Inst. Met.* 54 (1990) 1376–1381.
- [41] Q. Bi, W. Liu, J. Ma, J. Yang, Y. Pu, Q. Xue, *Tribol. Int.* 42 (2009) 1081–1087.
- [42] S. Ren, J. Meng, J. Wang, J. Lu, S. Yang, *Wear* 269 (2010) 50–59.
- [43] V. Rodriguez, J. Sukumaran, A.K. Schlarb, P. De Baets, *Tribol. Int.* 103 (2016) 45–57.
- [44] Y.H. Yau, M.A. Streicher, *Corrosion* 47 (1991) 352–359.
- [45] U.K. Mudali, R. Kaul, S. Ningshen, P. Ganesh, A.K. Nath, H.S. Khatak, B. Raj, *Mater. Sci. Technol.* 22 (2006) 1185–1192.
- [46] S. Fajardo, I. Llorente, J.A. Jiménez, N. Calderón, D. Herrán-Medina, J.M. Bastidas, J. Ressa, D.M. Bastidas, *Appl. Surf. Sci.* 513 (2020) 145852.
- [47] B.Z. Sun, X.M. Zuo, X.Q. Cheng, X.G. Li, *npj Mater. Degrad.* 4 (2020) 37.
- [48] X. Zhang, L. Lin, Y. Xia, Q. Tan, Z. Zhu, Q. Mao, M. Zhou, *Tunnelling and Underground Space Technology* 82 (2018) 346–357.
- [49] J.C. Rawers, J.S. Dunning, G. Asai, R.P. Reed, *Metall. Trans. A* 23 (1992) 2061–2068.
- [50] H. Luo, X. Wang, C. Dong, K. Xiao, X. Li, *Corros. Sci.* 124 (2017) 178–192.
- [51] H. Tao, C. Zhou, Y. Zheng, Y. Hong, J. Zheng, L. Zhang, *Corros. Sci.* 154 (2019) 268–276.
- [52] S. Mischler, A. Spiegel, M. Stemp, D. Landolt, *Wear* 251 (2001) 1295–1307.
- [53] A. Van Herpen, B. Reynier, C. Phalippou, *Wear* 249 (2001) 37–49.

Springer Nature or its licensor (e.g. a society or other partner) holds exclusive rights to this article under a publishing agreement with the author(s) or other rightsholder(s); author self-archiving of the accepted manuscript version of this article is solely governed by the terms of such publishing agreement and applicable law.